

Effect of overheating-induced minor addition on Zr-based metallic glasses

Fu Yang(杨福), Zhenxing Bo(薄振兴), Yao Huang(黄瑶), Yutian Wang(王雨田), Boyang Sun(孙博阳), Zhen Lu(鲁振), Baoan Sun(孙保安), Yanhui Liu(柳延辉), Weihua Wang(汪卫华), and Mingxiang Pan(潘明祥)

Citation: Chin. Phys. B, 2024, 33 (**3**): 036401. DOI: 10.1088/1674-1056/ad1823
Journal homepage: http://cpb.iphy.ac.cn; http://iopscience.iop.org/cpb

What follows is a list of articles you may be interested in

A group of ductile metallic glasses prepared by modifying local structure of icosahedral quasicrystals

Qi Qiao(乔琪), Ji Wang(王吉), Zhengqing Cai(蔡正清), Shidong Feng(冯士东), Zhenqiang Song(宋贞强), Benke Huo(霍本科), Zijing Li(李子敬), and Li-Min Wang(王利民)

Chin. Phys. B, 2023, 32 (**11**): 116401. DOI: 10.1088/1674-1056/ace823

Crystallization evolution and relaxation behavior of high entropy bulk metallic glasses using microalloying process

Danhong Li(李丹虹), Changyong Jiang(江昌勇), Hui Li(栗慧), and Mahander Pandey

Chin. Phys. B, 2021, 30 (**6**): 066401. DOI: 10.1088/1674-1056/abd92c

Internal friction behavior of $Zr_{59}Fe_{18}Al_{10}Ni_{10}Nb_3$ metallic glass under different aging temperatures

Israa Faisal Ghazi, Israa Meften Hashim, Aravindhan Surendar, Nalbiy Salikhovich Tuguz, Aseel M. Aljeboree, Ayad F. Alkaim, and Nisith Geetha

Chin. Phys. B, 2021, 30 (**2**): 026401. DOI: 10.1088/1674-1056/abc14f

Thermal effects and evolution of the defect concentration based on shear modulus relaxation data in a Zr-based metallic glass

Qi Hao(郝奇), Ji-Chao Qiao(乔吉超), E V Goncharova, G V Afonin, Min-Na Liu(刘敏娜), Yi-Ting Cheng(程怡婷), V A Khonik

Chin. Phys. B, 2020, 29 (**8**): 086402. DOI: 10.1088/1674-1056/ab969c

Effect of Sn and Al additions on the microstructure and mechanical properties of amorphous Ti-Cu-Zr-Ni alloys

Fu-Chuan Chen(陈福川), Fu-Ping Dai(代富平), Xiao-Yi Yang(杨霄熠), Ying Ruan(阮莹), Bing-Bo Wei(魏炳波)

Chin. Phys. B, 2020, 29 (**6**): 066401. DOI: 10.1088/1674-1056/ab8628

RAPID COMMUNICATION

Effect of overheating-induced minor addition on Zr-based metallic glasses

Fu Yang(杨福)[1,2], Zhenxing Bo(薄振兴)[1,2], Yao Huang(黄瑶)[1,2], Yutian Wang(王雨田)[1,2], Boyang Sun(孙博阳)[1,2], Zhen Lu(鲁振)[1], Baoan Sun(孙保安)[1,4], Yanhui Liu(柳延辉)[1,2,3,†], Weihua Wang(汪卫华)[1,3,4], and Mingxiang Pan(潘明祥)[1,3,4,‡]

[1] *Institute of Physics, Chinese Academy of Sciences, Beijing* 100190, *China*
[2] *Center of Materials Science and Optoelectronics Engineering, University of Chinese Academy of Sciences, Beijing* 100049, *China*
[3] *School of Physical Sciences, University of Chinese Academy of Sciences, Beijing* 100049, *China*
[4] *Songshan Lake Materials Laboratory, Dongguan* 523808, *China*

(Received 30 November 2023; revised manuscript received 20 December 2023; accepted manuscript online 22 December 2023)

Melt treatment is well known to have an important influence on the properties of metallic glasses (MGs). However, for the MGs quenched from different melt temperatures with a quartz tube, the underlying physical origin responsible for the variation of properties remains poorly understood. In the present work, we systematically studied the influence of melt treatment on the thermal properties of a $Zr_{50}Cu_{36}Al_{14}$ glass-forming alloy and unveiled the microscopic origins. Specifically, we quenched the melt at different temperatures ranging from $1.1T_l$ to $1.5T_l$ (T_l is the liquidus temperature) to obtain melt-spun MG ribbons and investigated the variation of thermal properties of the MGs upon heating. We found that glass transition temperature, T_g, increases by as much as 36 K, and the supercooled liquid region disappears in the curve of differential scanning calorimetry when the melt is quenched at a high temperature up to $1.5T_l$. The careful chemical analyses indicate that the change in glass transition behavior originates from the incorporation of oxygen and silicon in the molten alloys. The incorporated oxygen and silicon can both enhance the interactions between atoms, which renders the cooperative rearrangements of atoms difficult, and thus enhances the kinetic stability of the MGs.

Keywords: metallic glass, thermal properties, melt treatment, overheating, oxygen content

PACS: 64.70.pe, 63.50.Lm, 65.60.+a, 81.05.Kf **DOI:** 10.1088/1674-1056/ad1823

1. Introduction

Metallic glasses (MGs), rapidly quenched from molten alloy liquids, are often considered frozen liquids because the solid MGs inherit to some extent the liquid structure.[1] The disordered atomic structures of MGs result in many unachievable properties with crystalline alloys, such as high strength,[2–6] large elastic limit,[7–9] and thermal-plastic formability.[10–12] Because the atomic structures of MGs are believed to depend on thermal history,[13] many efforts have been devoted to the investigation on the effects of melt treatment, in particular, overheating and quenching temperature, T_q, on thermal stability,[14–30] glass formation ability (GFA),[31–36] magnetic[37–40] and mechanical properties,[27,28,41–44] and corrosion resistance.[45,46] Substantial changes in properties have been experimentally observed. However, the trend of these changes is often inconsistent in reported investigations. For example, in some investigations overheating the molten alloy to a high quenching temperature could lead to higher glass transition temperature T_g and crystallization temperature T_x of the obtained MGs,[14,16–18,21–25,28,47,48] while decreased T_x with increasing T_q was reported in other investigations when the molten alloy was overheated.[25,26] In addition, it was found that glass transition and supercooled liquid region (SLR) disappear when glass-forming alloys are overheated and quenched from high T_q.[25] Nonetheless, the persistence of distinct glass transition and SLR in the MGs quenched from high T_q was also reported.[14–24] The variation of MG properties has been predominately ascribed to the evolution of locally ordered clusters and precipitation of high-temperature phases when the molten alloy is overheated and quenched at different T_q. The MGs obtained from a high T_q were assumed to have a more homogenous structure. However, the investigations by MD simulations suggested that the effect of T_q on the formation of MG is negligible.[49]

For the investigations on the effect of melt treatment, Zr-based MGs were often chosen as model materials because their superior GFA allows changes of T_q in a wide temperature range.[3,50] Additionally, induction melting in a quartz tube was usually used to overheat the molten alloys because the temperature measurement is more convenient during overheating. However, Zr has a large chemical activity with oxygen at high temperatures, and a large amount of oxygen has been detected in the MGs quenched from high T_q through in-

†Corresponding author. E-mail: yanhui.liu@iphy.ac.cn
‡Corresponding author. E-mail: panmx@iphy.ac.cn

© 2024 Chinese Physical Society and IOP Publishing Ltd

duction melting.[31,48] Although it is well known that minor additions have a substantial impact on the formation and properties of MGs,[51] the influence of oxygen has not received sufficient attention. As a consequence, it remains elusive whether the property variation of the overheated Zr-based MGs originates from a more homogenous structure or the incorporation of elements such as oxygen.

In this work, we systematically investigate the effect of T_q on the thermal properties, crystallization kinetics, relaxation behaviors, and mechanical properties of $Zr_{50}Cu_{36}Al_{14}$ MG ribbons. We found that with the increase of T_q during the melt spinning process, the properties of $Zr_{50}Cu_{36}Al_{14}$ MG ribbons undergo significant changes. Through chemical composition analysis, it turns out that the effect of T_q actually roots from the redox reaction between molten alloy and quartz tubes, which renders silicon and oxygen elements incorporated into $Zr_{50}Cu_{36}Al_{14}$ MG ribbons. These results can enable us to comprehensively understand the role of melt treatment on the properties of MGs, and provide some experimental foundation for the control of the structure–performance relationship in glass-forming alloys.

2. Experiment

Master alloys with the nominal compositions (at.%) of $Zr_{50}Cu_{36}Al_{14}$ and $Au_{50}Cu_{25.5}Ag_{7.5}Si_{17}$ were prepared by arc-melting a mixture of pure metals in a Ti-gettered argon atmosphere. The purities of the raw materials are Zr 99.9%, Cu 99.99%, Al 99.999%, Au 99.999%, Ag 99.999%, and Si 99.999% (all in wt.%), respectively. In order to achieve homogeneity in composition, each ingot was remelted more than six times. Melt spinning was used to prepare MG ribbons. The preparation was carried out under the protection of a high-purity argon atmosphere after the vacuum reached 8×10^{-4} Pa. The ingots were heated by induction heating in quartz tubes to a specific T_q and then immediately quenched the melt at that T_q. The MG ribbons were obtained by quenching the molten liquid at different temperatures. We used a new quartz tube for every MG ribbon. The molten liquid temperature was measured by a radiation thermometer with an accuracy of $\pm$20 K. The quartz-tube nozzle hole diameter, the copper wheel rotation speed, and ejection pressure difference were set to 0.4 mm, 2400 rpm, and 0.2 MPa, respectively. The average oxygen contents were measured by a high-temperature thermal decomposition analyzer (Yanrui NO-330) with an accuracy of 1 wt. ppm for oxygen. The compositions of the MG ribbons were analyzed by employing inductively coupled plasma–atomic emission spectroscopy (ICP–AES).

The x-ray diffraction (XRD) analysis was carried out by using a Bruker D8 Advance diffractometer with a Cu K_α source. A high-resolution transmission electron microscope (HRTEM) was also used to characterize the structure of MG ribbons obtained from different T_q. The HRTEM specimens were prepared by ion milling with 3 kV Ar ions. HRTEM observation was carried out by a transmission electron microscope (TEM, JEM-2100PLUS, JEOL, 200 kV) with a field emission gun.

A Perkin–Elmer differential scanning calorimetry (DSC) 8000 was employed to examine the thermodynamic properties of the MG ribbons at a heating rate of 20 K·min^{-1} with 20 mL·min^{-1} flowing pure argon to prevent possible surface oxidation. The melting points and liquidus temperatures were measured by a differential thermal analyzer (Netzsch DSC 404C). The dynamic mechanical analysis (DMA) measurements were performed on a TA DMA Q800 in a temperature-ramp mode under the frequency of 1 Hz and an amplitude of 10 μm. The stress relaxation measurement was performed through DMA at a temperature of $0.8T_g$ and a tensile strain of 0.7%.

Nanoindentation measurements were carried out on Hysitron TI980 using a calibrated diamond Berkovich indenter with a nominal tip radius of curvature of 50 nm under the load-controlled mode. The tests were conducted by using partial unload mode, which included 33 loading–unloading cycles from 500 μN to 10000 μN at room temperature. Each cycle comprised of loading, holding, and unloading. The loading time, hold time, and unloading time were all one second. The unloading fraction parameter which controlled the percentage of unloading for each unloading segment was set to 0.5.

3. Results and discussion

Figure 1(a) shows XRD patterns of $Zr_{50}Cu_{36}Al_{14}$ MG ribbons obtained from different T_q. It can be seen that there only exist broad diffraction peaks without any sharp crystal diffraction peaks within the resolution of XRD, indicating the amorphous structure of the MGs. In order to exclude the possibility of nanocrystalline precipitation in the MG ribbons, we also characterized the structure of the MGs through HRTEM and selected area electron diffraction (SAED). Figures 1(b)–1(f) show the HRTEM images and SAED patterns of $Zr_{50}Cu_{36}Al_{14}$ MG ribbons prepared from $1.1T_l$ to $1.5T_l$ in turn. The maze-like patterns and diffraction halos confirm that the alloys are of disordered structure without the formation of nanocrystals.

Figure 2(a) shows the DSC curves for $Zr_{50}Cu_{36}Al_{14}$ MG ribbons prepared from various T_q. As can be seen from the DSC curves, the calorimetric T_g gradually shifts towards a higher value when T_q increases from $1.1T_l$ to $1.4T_l$. However, when the MG ribbon is quenched from $1.5T_l$, neither glass transition nor SLR could be observed. This phenomenon is consistent with the previous report,[25] and the disappearance of glass transition and SRL was ascribed to the change of atomic configurations from densely-coordinated to loosely-

coordinated atomic packing. Whereas, it suggested that the phenomenon could be observed only when T_q is 700 K above T_l.[25] In our case, the phenomenon takes place at a lower T_q, i.e., the T_q is only 400–500 K higher than T_l. According to previous investigations, distinct glass transition and SLR should be observable in our case.[14–24]

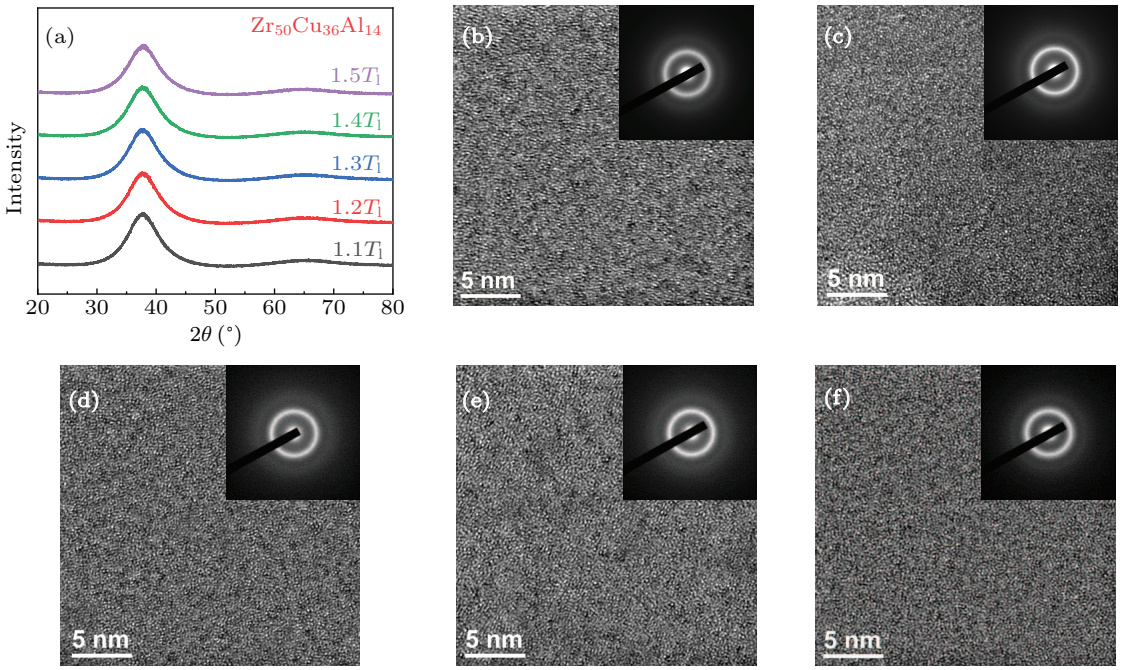


Fig. 1. Structural characterization. (a) XRD patterns of $Zr_{50}Cu_{36}Al_{14}$ melt-spun MG ribbons prepared by melt spinning from different quenching temperatures (T_q) ranging from $1.1T_l$ to $1.5T_l$. HRTEM and SAED images for the $Zr_{50}Cu_{36}Al_{14}$ melt-spun MG ribbons quenched from (b) $1.1T_l$, (c) $1.2T_l$, (d) $1.3T_l$, (e) $1.4T_l$, and (f) $1.5T_l$.

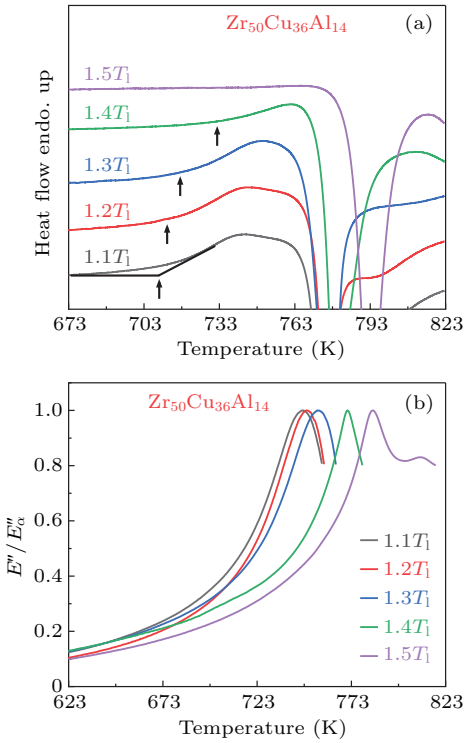


Fig. 2. The variation of glass transition. (a) Glass transition characterized by DSC for $Zr_{50}Cu_{36}Al_{14}$ melt-spun MG ribbons prepared from different T_q. The heating rate is 20 K/min. T_g is marked out with the arrows and defined from the onset of the transition as indicated by the intersection of the black lines. (b) The normalized loss modulus E''/E''_α at frequency $f = 1$ Hz and heating rate of 3 K/min. The peak temperature is taken as the kinetic glass transition temperature T_α.

To confirm the disappearance of glass transition, we conducted DMA measurements. In contrast to other thermodynamic methods such as DSC and thermal mechanical analysis, DMA is more sensitive in detecting the occurrence of various atomic motions and transformations, and the glass transition can be revealed as a dynamic process at the dynamical glass transition temperature T_α. Figure 2(b) illustrates the temperature dependence of the normalized loss modulus, E''/E''_α, for $Zr_{50}Cu_{36}Al_{14}$ MG ribbons. One can see that T_α increases from 748 K to 784 K when T_q varies from $1.1T_l$ to $1.5T_l$. This indicates that higher energy is required to activate the cooperative rearrangement of atoms in the MGs quenched from higher melt temperatures. The measurement results by DMA are consistent with those by DSC. In both cases, the glass transition temperature shifts to a higher value when T_q is increased. Furthermore, we prepared $Zr_{50}Cu_{36}Al_{14}$ MG ribbons at the same T_q but at different spinning speeds of the copper wheel. As shown in Fig. S1, T_α remains unchanged. This suggests that the cooling rate has a negligible contribution to the increase of T_α. It is worth mentioning that the MG ribbon obtained from the high T_q of $1.5T_l$ still shows a distinct dynamic glass transition.

In general, the enhanced kinetic stability of MGs can be interpreted from the perspective of potential energy landscape (PEL).[52–55] Hence, we probed the distribution of relaxation energy barriers for the $Zr_{50}Cu_{36}Al_{14}$ MG ribbons. Figure 3(a) shows the isothermal stress relaxation responses

of $Zr_{50}Cu_{36}Al_{14}$ MG ribbons. Figure 3(b) presents the distributions of relaxation energy barriers derived from the stress relaxation curves according to the activation energy spectrum model.[56,57] It can be seen that for the MG with a higher T_q, the energy barrier distribution shifts towards a higher value. This suggests that the MGs quenched from higher temperatures are located in the deeper basins in PEL. Figure 3(c) shows the apparent relaxation time, τ, obtained by fitting the stress relaxation curves with the KWW equation.[58,59] As can be seen, τ increases from 1209 ± 28 s to 2812 ± 45 s when T_q increases from $1.1T_l$ to $1.5T_l$. This indicates that the atomic mobility in $Zr_{50}Cu_{36}Al_{14}$ MG ribbons reduces with the rise of T_q.

In addition, the ease of glass transition which involves cooperative rearrangement of atoms[60] can be quantified by the apparent activation energy (E_g). Figure 3(d) shows the DSC traces with the heating rates ranging from 20 K/min to 140 K/min for the $Zr_{50}Cu_{36}Al_4$ MG ribbon quenched at $1.3T_l$. It can be seen that T_g and the temperature of the first crystallization peak (T_{xp}) shift to higher temperatures with the increase of the heating rate, which arises from the involvement of thermal activation in these kinetic processes. The activation energy for glass transition and crystallization can be obtained through the Kissinger equation[57,61]

$$\ln\frac{\Phi}{T^2} = C - \frac{E^*}{RT},$$

where Φ is the heating rate, C is a constant, R is the ideal gas constant, and E^* is the apparent activation energy. As shown in Fig. 3(e), the activation energy increases remarkably with the increase of quenching temperatures. For example, E_g is enhanced from 660 ± 48 kJ·mol^{-1} to 991 ± 52 kJ·mol^{-1} when T_q increases from $1.1T_l$ to $1.5T_l$. It should be noted that the E_g value for the MG prepared from $1.1T_l$ is in line with that reported in the literature.[62] We also estimated the fragility (m) of the $Zr_{50}Cu_{36}Al_4$ MG ribbons quenched from different temperatures (Fig. 3(f)). As can be seen, with the increase of T_q, the MGs become more and more fragile.

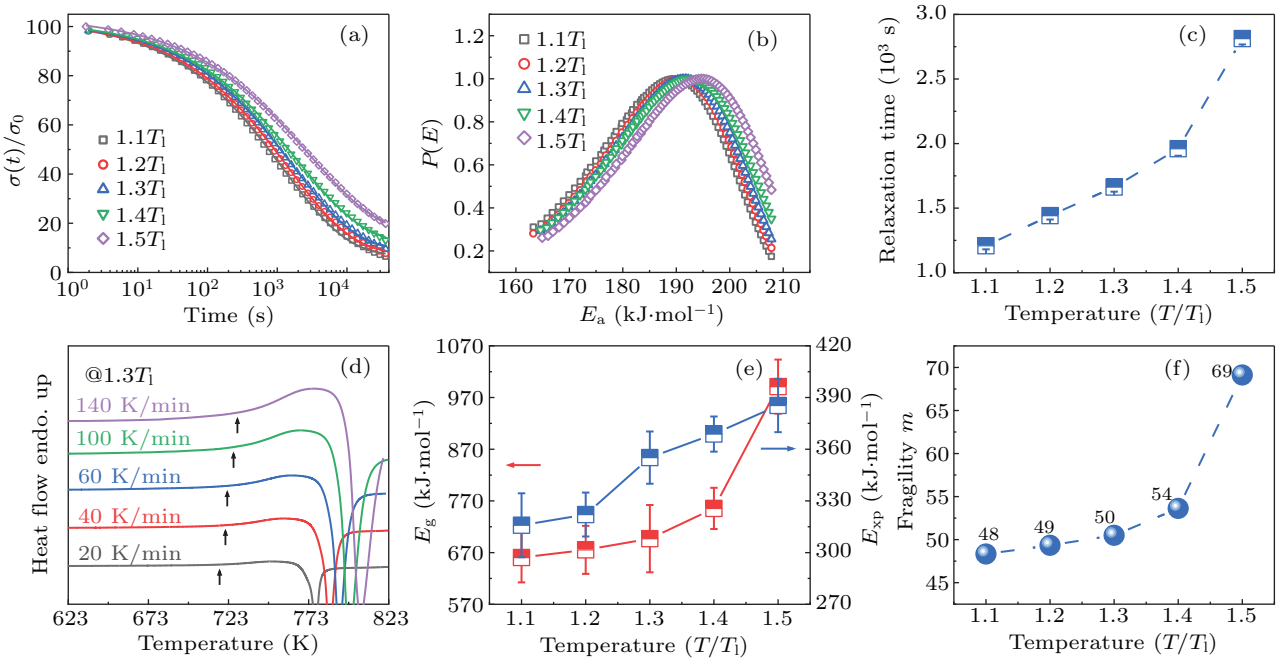


Fig. 3. The evolution of atom motion in solid glass and supercooled liquid. (a) The stress relaxation curves of $Zr_{50}Cu_{36}Al_{14}$ MG ribbons prepared from different T_q. In the stress relaxation experiments, a tensile strain $\varepsilon = 0.7\%$ is applied to the MG ribbons at $0.8T_g$ (619 K). Solid lines are fittings to the data. (b) Normalized activation energy spectra $P(E)$. (c) Variation of relaxation time τ as a function of T_q. (d) DSC traces for the $Zr_{50}Cu_{36}Al_{14}$ MG ribbons quenched from $1.3T_l$. The heating rates range from 20 K/min to 140 K/min. T_g is marked out with the arrows. (e) Activation energies of glass transition and crystallization as a function of T_q for $Zr_{50}Cu_{36}Al_{14}$ MG ribbons. The temperature of the first crystallization peak is taken as T_{xp}. (f) Dependence of fragility m of $Zr_{50}Cu_{36}Al_{14}$ MG ribbons on T_q.

We also investigated the influence of T_q on the crystallization kinetics of the $Zr_{50}Cu_{36}Al_4$ MG. The MG ribbons prepared from $1.1T_l$, $1.4T_l$, and $1.5T_l$ were heated to their respective T_x, and then the evolution of crystallization phases with isothermal time was investigated (Fig. 4). We found that the MG ribbons quenched from $1.4T_l$ and $1.5T_l$ can maintain the amorphous structure if they are heated to their corresponding T_x and immediately cooled down to room temperature (see Figs. 4(b) and 4(c)). In contrast, the diffraction hump is distorted for the MG ribbon quenched at $1.1T_l$, suggesting the formation of nanocrystals in the alloy. After isothermal annealing for 2 min at T_x, sharp diffraction peaks emerge in all three alloys, indicating the precipitation of crystalline phases. For the MG prepared from $1.1T_l$, the crystalline phases are identified to be $CuZr_2$, Al_3Zr, and $AlCu_2Zr$ after isothermal annealing for 2 min. Prolonged annealing leads to the formation of $AlZr_3$ and $AlCu_4$ phases. However, for the MGs prepared from $1.4T_l$ and $1.5T_l$, the crystalline phases do not

change with annealing time. The crystalline phases are identified to be mainly $Cu_{10}Zr_7$, $AlZr_2$, and Al_3Zr_2, respectively. These observations manifest that the variation of T_q can lead to different crystallization processes, which probably depend on the evolution of the structures, types, and quantity of local atomic clusters with the increase of melt temperatures.

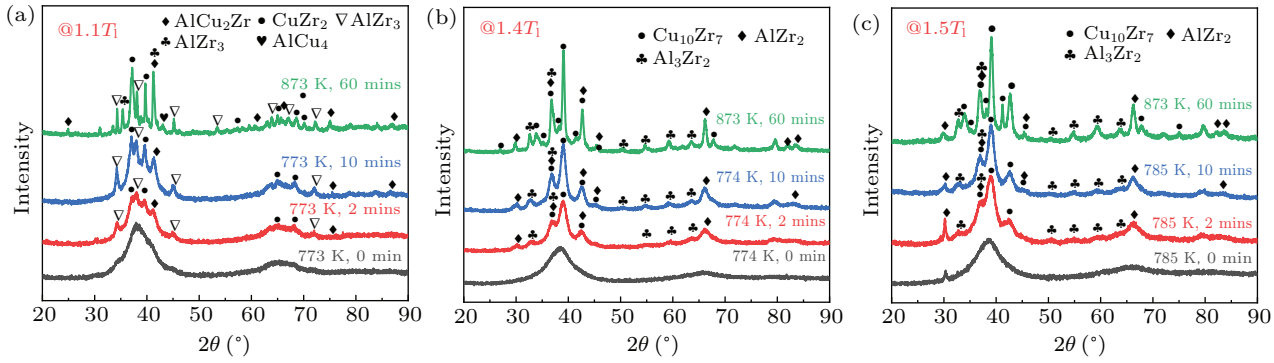


Fig. 4. The crystallization and phase formation. XRD patterns for $Zr_{50}Cu_{36}Al_{14}$ melt-spun MG ribbons prepared from (a) $1.1T_l$, (b) $1.4T_l$, and (c) $1.5T_l$.

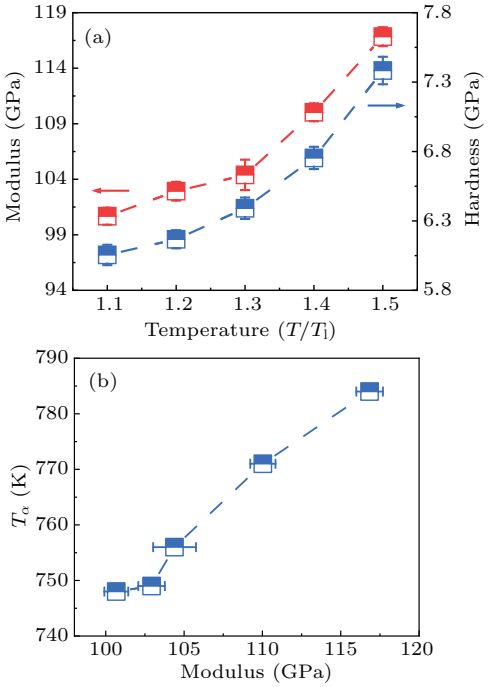


Fig. 5. The modulus and hardness characterization. (a) The average modulus E and hardness depend on T_q for a series of $Zr_{50}Cu_{36}Al_{14}$ melt-spun MG ribbons determined by nanoindentation measurements. The error bars were obtained by standard deviation from the statistical average value of six test sites in each alloy. (b) Variation of T_α as a function of E.

We utilized nanoindenter to measure the modulus E and hardness. The E and hardness dependence on T_q is illustrated in Fig. 5(a) for $Zr_{50}Cu_{36}Al_{14}$ MG ribbons. With the increase of T_q from $1.1T_l$ to $1.5T_l$, E increases from 100.67 ± 0.76 GPa to 116.84 ± 0.85 GPa. The hardness also increases, i.e., from 6.05 ± 0.07 GPa to 7.38 ± 0.10 GPa. Figure 5(b) shows T_α as a function of E for $Zr_{50}Cu_{36}Al_{14}$ MG ribbons quenched from different temperatures. It can be seen that T_α increases monotonically with E. Those results are in line with reported results that T_g and hardness are directly proportional to E.[54] One can see that the MG ribbons obtained from higher T_q show higher T_α, hardness, and E.

The variation in the properties of MGs with T_q has been reported in previous literature. In the majority of past studies, the structural origin of property changes is generally interpreted as the gradual dissipations of local atomic clusters or the nucleation cores at high melt temperatures so that less ordered clusters are retained in MGs after quenching.[14,21,22,24,25] Nevertheless, it has been reported that the elevation of T_q will lead to the increase of oxygen content in the alloy.[31,48] To understand the T_q-dependence of property changes, we carefully analyzed the chemical compositions of the MG ribbons quenched from different melt temperatures. Figure 6(a) shows the dependence of the analytical oxygen content on T_q for a series of $Zr_{50}Cu_{36}Al_{14}$ MG ribbons. It can be seen that the oxygen content in MG ribbons increases monotonically with the increase of T_q. This invokes us to scrutinize the correlation between the property changes and the variation of oxygen content. We gathered data on the change of T_g and oxygen content in Zr-based MGs fabricated at different T_q from the literature, and found that the greater the extent of variation in oxygen content, the more pronounced the magnitude of change in T_g (see Fig. S2).[25] It is known that the constituents in Zr-based alloy have a chemical affinity with oxygen, in particular, at high temperatures.[31] For example, the heat of formation for ZrO_2 is about 1100 kJ·mol^{-1}, larger than that of SiO_2 (908 kJ·mol^{-1}), which is the main component of quartz tubes. Thermodynamically, O can be absorbed by Zr through the redox reaction at high temperatures.[31] Moreover, we found that the content of Zr does slightly decrease with the increase of T_q, and there exist 0.76 at.% and 1.24 at.% Si in the MG ribbons quenched from $1.4T_l$ and $1.5T_l$, respectively (as shown in Table 2). This indicates that the incorporation of oxygen in the Zr–Cu–Al alloys is associated with the reaction of molten alloy with SiO_2. This is supported by the chemical analysis of a Fe-based MG, as shown in Table S4. We found that the variation of oxygen content is ignorable between $Fe_{78}Si_9B_{13}$ ingot and the ribbon quenched from a higher temperature (1576 K).

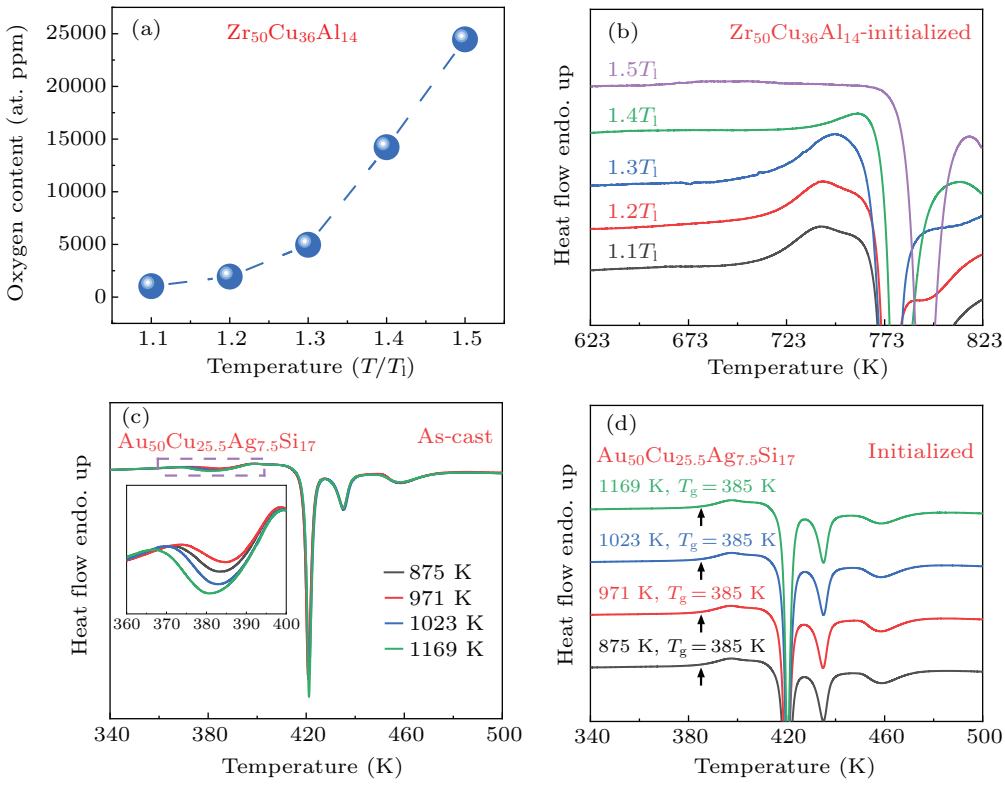


Fig. 6. Confirming oxygen as the dominant factor for the change of thermal properties. (a) The T_q-dependence of oxygen content for the $Zr_{50}Cu_{36}Al_{14}$ melt-spun MG ribbons. (b) DSC curves of $Zr_{50}Cu_{36}Al_{14}$ melt-spun MG ribbons after initialized by heating to the supercooled liquid region. (c) DSC curves of $Au_{50}Cu_{25.5}Ag_{7.5}Si_{17}$ melt-spun MG ribbons prepared by melt spinning from different T_q of 875 K, 971 K, 1023 K, and 1169 K. The inset in (c) is the enlargement of the DSC curves related to the relaxation enthalpy regions. (d) DSC traces of $Au_{50}Cu_{25.5}Ag_{7.5}Si_{17}$ melt-spun MG ribbons initialized by heating to 405 K.

Table 1. Calorimetric glass transition temperature (T_g), kinetic glass transition temperature (T_α), onset crystallization temperature (T_x), the temperature of the first crystallization peak (T_{xp}), the width of the supercooled liquid region (ΔT_x), melting point (T_m) and liquidus temperature (T_l) of $Zr_{50}Cu_{36}Al_{14}$ MG ribbons prepared from different temperatures.

Samples	T_α (K)	T_g (K)	T_x (K)	ΔT_x (K)	T_{xp} (K)	T_m (K)	T_l (K)
$1.1T_l$	748	710	773	63	775	1126	1151
$1.2T_l$	749	712	775	63	777	1125	1150
$1.3T_l$	756	717	774	57	777	1125	1148
$1.4T_l$	771	732	774	42	780	1123	1144
$1.5T_l$	784	–	785	–	793	1130	1150

Table 2. The compositions of $Zr_{50}Cu_{36}Al_{14}$ melt-spun MG ribbons determined by chemical analysis.

Samples	Zr (at.%)	Cu (at.%)	Al (at.%)	Si (at.%)	Hf (at.%)	O (at. ppm)
$1.1T_l$	49.71	35.79	13.87	–	0.52	1035
$1.2T_l$	49.10	36.26	13.92	–	0.53	1941
$1.3T_l$	48.73	36.34	13.91	–	0.53	4961
$1.4T_l$	47.88	35.71	13.71	0.76	0.52	14227
$1.5T_l$	47.26	34.91	13.66	1.24	0.51	24457

In order to further confirm that the property changes of the $Zr_{50}Cu_{36}Al_{14}$ MG ribbons prepared from different T_q result from the redox reaction between molten alloy and quartz tubes, we prepared $Au_{50}Cu_{25.5}Ag_{7.5}Si_{17}$ MG ribbons which are chemically inert.[63] As in the case of $Zr_{50}Cu_{36}Al_{14}$ MG, the $Au_{50}Cu_{25.5}Ag_{7.5}Si_{17}$ MG ribbons were prepared from various T_q ranging from 875 K to 1169 K, which are 220–520 K higher than T_l ($T_l = 655$ K) (as shown in Figs. 6(c) and 6(d)). To eliminate the history-dependence and better compare the thermal properties of different samples, the as-quenched MG ribbons were initialized. After initialization, DSC measurements on the Au-based MG indicate that the T_g and T_x remain essentially unchanged when T_q is varied.[64] In comparison, the T_g and T_x of $Zr_{50}Cu_{36}Al_{14}$ MG after initialization still maintain the difference with the elevation of T_q (Fig. 6(b)). These results clearly demonstrate that the effect of overheating temperature on the variation of T_g and T_x is negligible in $Zr_{50}Cu_{36}Al_{14}$ MG ribbons. Therefore, it is considered that the property changes for $Zr_{50}Cu_{36}Al_{14}$ MGs with the variation of T_q highly possibly arise from the reaction of the molten alloy with quartz tubes, rather than the dissipation of locally ordered clusters or high-temperature crystalline phases.

In the present system, the atomic radii of components are Zr = 2.06 Å, Cu = 1.45 Å, Al = 1.18 Å, Si = 1.11 Å, and O = 0.48 Å. Compared with the original constituents, Si and O are of smaller atom sizes. Therefore, the incorporation of Si and O elements will increase the degree of atomic size difference between the alloying elements. At the same time, smaller atoms are prone to occupy interstitial spaces in the alloy, improving the local packing efficiency. Furthermore, the Si and O elements possess large mixing heat with other constituent elements. For example, the mixing heat values of Zr–Si, Cu–Si, Al–Si, Zr–Cu, Zr–Al, Al–Cu are −84 kJ/mol, −19 kJ/mol, −19 kJ/mol, −23 kJ/mol,

−44 kJ/mol, and −1 kJ/mol, respectively.[65] These large negative values of mixing heat enhance the atomic interactions and promote chemical short-range order, which can render long-range atomic diffusion difficult. It has been reported that the addition of oxygen can result in the formation of Zr–O octahedral structure with an O atom surrounded by six Zr atoms.[66,67] The bond energy of Zr–Zr, Cu–Cu, Al–Al, and Zr–O is 298.2 ± 0.1 kJ·mol^{-1}, 182 ± 2.5 kJ·mol^{-1}, 264.3 ± 0.5 kJ·mol^{-1}, and 766.1 ± 10.6 kJ·mol^{-1}, respectively.[68] It can be seen that the Zr–O atomic pair possesses the highest bond energy, indicating that the atomic bonding in the Zr–O local clusters is stronger than that in the other clusters. In a word, the addition of Si and O elements will facilitate the formation of local atomic clusters with stronger interatomic interaction. To activate the diffusion of these clusters, higher energy is required. With the increase of T_q, more Si and O elements are reacted into the MG ribbons, so the atomic cooperative rearrangements are delayed to higher temperatures, leading to an elevated T_g (or T_α) upon heating, a higher E, and hardness. In addition, the gradual increase of local atomic clusters, especially for Zr–O local clusters, will lead to the reduction of preferentially activated atoms involved in glass transition. This is reflected in the signal intensity of glass transition in DSC curves. This may be the reason why glass transition and SLR disappeared in the DSC curves for the MGs quenched from $1.5T_l$. On top of that, the structure, type, and quantity of local atomic clusters will evolve with the variation of Si and O contents, which causes the variation in crystallization kinetics and crystalline products with the elevation of T_q for $Zr_{50}Cu_{36}Al_{14}$ MG ribbons.

4. Conclusions

In summary, our results indicate that the variation of thermal properties of the Zr-based MG ribbons obtained by overheating arises from the incorporation of oxygen and silicon due to the reaction of the molten alloy with quartz tubes. We found that T_g monotonically increases with the elevation of T_q. For the MGs quenched from $1.5T_l$, the SLR disappears and the intensity of glass transition weakens upon heating, at which the MGs should have a distinct glass transition and SLR according to reported literature. Through chemical analysis, we confirmed that the variation of thermal properties caused by overheating mainly originates from the incorporation of oxygen and silicon elements. The oxygen and silicon are incorporated by the redox reaction between Zr elements and SiO_2 tubes during melting. Due to the smaller atom size and large negative mix heating values with other constituents, the incorporation of both Si and O can enhance the interatomic interaction, and even facilitate the formation of local atomic clusters with strong interatomic bonding. This slows down the motion of atoms and hinders the cooperative rearrangement of atoms during the glass transition process, and thus enhances the kinetic stability of the MGs. Since induction melting followed by injection casting is one of the most commonly used techniques for manufacturing BMGs including Zr-based BMGs, our results suggest that in some cases the reaction of quartz tubes with molten alloy should be taken into account, especially when correlating properties with MG composition.

Acknowledgements

The authors thank Zijian Wang, Rui Zhao, and Huaping Zhang for helpful discussions. The work was financially supported by the National Key Research and Development Program of China (Grant Nos. 2018YFA0703600, 2021YFA0716302, and 2021YFA0718703), the National Natural Science Foundation of China (Grant Nos. 51825104 and 52192602), and China Postdoctoral Science Foundation (Grant No. 2022T150691).

References

[1] Dyre J C 2006 *Rev. Mod. Phys.* **78** 953
[2] Inoue A, Shen B, Koshiba H, Kato H and Yavari A R 2003 *Nat. Mater.* **2** 661
[3] Wang W H, Dong C and Shek C H 2004 *Materials Science and Engineering: R: Reports* **44** 45
[4] Wang J, Li R, Hua N and Zhang T 2011 *J. Mater. Res.* **26** 2072
[5] Wang W H 2012 *Prog. Mater. Sci.* **57** 487
[6] Huo J, Li K, Zang B, Gao M, Wang L M, Sun B, Li M, Song L, Wang J Q and Wang W H 2022 *Chin. Phys. Lett.* **39** 046401
[7] Telford M 2004 *Materials Today* **7** 36
[8] Yi J, Xia X X, Zhao D Q, Pan M X, Bai H Y and Wang W H 2010 *Advanced Engineering Materials* **12** 1117
[9] Tian L, Cheng Y Q, Shan Z W, Li J, Wang C C, Han X D, Sun J and Ma E 2012 *Nat. Commun.* **3** 609
[10] Duan G, Wiest A, Lind M L, Li J, Rhim W K and Johnson W L 2007 *Adv. Mater.* **19** 4272
[11] Kumar G, Tang H X and Schroers J 2009 *Nature* **457** 868
[12] Schroers J 2010 *Adv. Mater.* **22** 1566
[13] Lu T, Liu S L, Sun Y H, Wang W H and Pan M X 2022 *Chin. Phys. Lett.* **39** 036401
[14] Fan C and Inoue A 1999 *Appl. Phys. Lett.* **75** 3644
[15] Mukherjee S, Zhou Z, Schroers J, Johnson W L and Rhim W K 2004 *Appl. Phys. Lett.* **84** 5010
[16] Lee J K, Bae D H, Kim W T and Kim D H 2004 *Materials Science and Engineering: A* **375–377** 332
[17] Fan C, Chen D, Liaw P K, Choo H, Benmore C, Siewenie J, Chen G L, Xie J X and Liu C T 2008 *Appl. Phys. Lett.* **93** 261905
[18] Zhu Z W, Zhang H F, Wang H, Ding B Z and Hu Z Q 2008 *J. Mater. Res.* **23** 2714
[19] Mu J A, Fu H M, Zhu Z W, Wang A M, Li H, Hu Z Q and Zhang H F 2010 *Advanced Engineering Materials* **12** 1127
[20] Zhao Y, Kou S, Suo H, Wang R and Ding Y 2010 *Materials & Design* **31** 1029
[21] Mao J, Zhang H F, Fu H M, Wang A M, Li H and Hu Z Q 2010 *J. Alloys Compd.* **496** 595
[22] Fan C, Liu C T, Chen G, Chen G, Chen D, Yang X, Liaw P K and Yan H G 2013 *Intermetallics* **38** 19
[23] Cui X, Zhang Q D, Li X Y and Zu F Q 2016 *Intermetallics* **73** 79
[24] Cui X, Zhang Q D, Li X Y and Zu F Q 2016 *J. Non-Cryst. Solids* **452** 336
[25] Wang X H, Inoue A, Kong F L, Zhu S L, Stoica M, Kaban I, Chang C T, Shalaan E, Al-Marzouki F and Eckert J 2016 *Acta Mater.* **116** 370
[26] Wang X H, Inoue A, Zhao J F, Kong F L, Zhu S L, Kaban I, Stoica M, Oswald S, Fan C, Shalaan E, Al-Marzouki F, Eckert J, Yin F X and Li Q 2018 *J. Alloys Compd.* **739** 1104
[27] Kumar G, Ohkubo T and Hono K 2009 *J. Mater. Res.* **24** 2353

[28] Mao J, Zhang H F, Fu H M, Wang A M, Li H and Hu Z Q 2010 *Materials Science and Engineering: A* **527** 981

[29] Cheng Q, Sun Y H, Orava J and Wang W H 2023 *Materials Today Physics* **31** 101004

[30] Chen C, Zhao R, Yin B, Chathoth S M, Inoue A, Embs J P, Zhang F, He Y, Li X, Chen Z, Zhang P and Shen B 2023 *J. Alloys Compd.* **967** 171691

[31] Mao J, Zhang H F, Fu H M, Wang A M, Li H and Hu Z Q 2009 *Advanced Engineering Materials* **11** 986

[32] Mu J, Fu H, Zhu Z, Wang A, Li H, Hu Z and Zhang H 2009 *Advanced Engineering Materials* **11** 530

[33] Zhu Z, Zhang H, Wang H, Ding B, Hu Z Q and Huang H 2009 *J. Mater. Res.* **24** 3108

[34] Liu J, Guo J, Hu X, Guo S, Meng W and Xiao Q 2013 *J. Alloys Compd.* **581** 671

[35] Jin Z, Cao F, Cao G, Zhang C, Qiu Z, Zhang L, Shen H, Jiang S, Huang Y, Ma M, Jürgen E and Sun J 2023 *Journal of Materials Research and Technology* **22** 3010

[36] Ouyang D L, Yan Y H, Chen S S, Huang D, Wang Z R, Cui X, Hu Q and Guo S 2023 *J. Non-Cryst. Solids* **603** 122118

[37] Luborsky F E and Liebermann H H 1981 *Materials Science and Engineering* **49** 257

[38] Manov V P, Popel S I, Buler P I, Manukhin A B and Komlev D G 1991 *Materials Science and Engineering: A* **133** 535

[39] Zhang S, Zhu W, Han C, Li W, Wang T, Chen C, Wei R, Wu S and Li F 2022 *Intermetallics* **151** 107741

[40] Gao H, Li Z, Zhou S, Zhang G and Cui N 2019 *Progress in Natural Science: Materials International* **29** 556

[41] Hu Y, Li J, Lin T and Zhou Y 2009 *J. Mater. Res.* **24** 3590

[42] Zhou X, Kou H, Wang J, Li J and Zhou L 2012 *Intermetallics* **28** 45

[43] Mohammadi Rahvard M, Tamizifar M and Boutorabi S M A 2018 *J. Non-Cryst. Solids* **491** 114

[44] Zhang X, Xu K, Yang X, Cui X, Bian B, Zhang X, Hou S and Chen J 2021 *AIP Advances* **11** 075105

[45] Du S, Li C, Pang S, Leng J and Geng H 2013 *Materials & Design* **47** 358

[46] Zhang X, Guo J, Liu H, Song Y, Xu L and Liu J 2016 *Materials & Design* **100** 217

[47] Zhu P, Li X, Zhang Q, Liu B, Ma Y and Zu F 2017 *J. Non-Cryst. Solids* **471** 175

[48] Cui X, Li J J, Qiao J C, Guo J, Zu F Q, Zhang X F, Meng X J, Bian B C and Zhang Q D 2020 *J. Non-Cryst. Solids* **543** 120100

[49] Mo J, Shen B, Wan Y, Zhou Z, Sun B and Liang X 2020 *J. Non-Cryst. Solids* **528** 119742

[50] Ashby M and Greer A 2006 *Scr. Mater.* **54** 321

[51] Wang W H 2007 *Prog. Mater. Sci.* **52** 540

[52] Angell C A 1995 *Science* **267** 1924

[53] Debenedetti P G and Stillinger F H 2001 *Nature* **410** 259

[54] Xue R J, Zhao L Z, Shi C L, Ma T, Xi X K, Gao M, Zhu P W, Wen P, Yu X H, Jin C Q, Pan M X, Wang W H and Bai H Y 2016 *Appl. Phys. Lett.* **109** 221904

[55] Zhang S, Wang W H and Guan P F 2021 *Chin. Phys. Lett.* **38** 016802

[56] Jiao W, Wen P, Peng H L, Bai H Y, Sun B A and Wang W H 2013 *Appl. Phys. Lett.* **102** 101903

[57] Kissinger H E 1956 *Journal of Research of the National Bureau of Standards* **57** 217

[58] Williams G and Watts D C 1970 *Transactions of the Faraday Society* **66** 80

[59] Williams G, Watts D C, Dev S B and North A M 1971 *Transactions of the Faraday Society* **67** 1323

[60] Stevenson J D, Schmalian J and Wolynes P G 2006 *Nat. Phys.* **2** 268

[61] Ligero R A, Vazquez J, Villares P and Jimenezgaray R 1989 *Mater. Lett.* **8** 6

[62] Han Z H, He L, Hou Y L, Feng J and Sun J 2009 *Intermetallics* **17** 553

[63] Zhang W, Guo H, Chen M W, Saotome Y, Qin C L and Inoue A 2009 *Scr. Mater.* **61** 744

[64] Zhao Y, Shang B, Zhang B, Tong X, Ke H, Bai H and Wang W H 2022 *Science Advances* **8** eabn3623

[65] Takeuchi A and Inoue A 2005 *Mater. Trans.* **46** 2817

[66] Altounian Z, Batalla E, Strom-Olsen J O and Walter J L 1987 *J. Appl. Phys.* **61** 149

[67] Wang Z Y, Huang L, Yue G Q, Shen B, Dong F, Zhang R J, Zheng Y X, Wang S Y, Wang C Z, Kramer J, Ho K M and Chen L Y 2016 *J. Phys. Chem. B* **120** 9223

[68] Haynes W M 2016 *CRC Handbook of Chemistry and Physics*, 97th edn., Vol. 9 (Boca Raton: CRC press) pp. 73–77